2016

Flight Mechanics and Control of Escape Manoeuvres in Hummingbirds. II. Aerodynamic Force Production, Flight Control and Performance Limitations

Bo Cheng
The Pennsylvania State University

Bret W. Tobalske
University of Montana, Missoula

Donald R. Powers
George Fox University, dpowers@georgefox.com

Tyson L. Hedrick
University of North Carolina at Chapel Hill

Yi Wang
Purdue University

See next page for additional authors

© 2016. Published by The Company of Biologists Ltd | Journal of Experimental Biology (2016) 219, 3532-3543 doi:10.1242/jeb.137570

RESEARCH ARTICLE

Flight mechanics and control of escape manoeuvres in hummingbirds. II. Aerodynamic force production, flight control and performance limitations

Bo Cheng[1,*], Bret W. Tobalske[2], Donald R. Powers[3], Tyson L. Hedrick[4], Yi Wang[5], Susan M. Wethington[6], George T.-C. Chiu[5] and Xinyan Deng[5]

ABSTRACT

The superior manoeuvrability of hummingbirds emerges from complex interactions of specialized neural and physiological processes with the unique flight dynamics of flapping wings. Escape manoeuvring is an ecologically relevant, natural behaviour of hummingbirds, from which we can gain understanding into the functional limits of vertebrate locomotor capacity. Here, we extend our kinematic analysis of escape manoeuvres from a companion paper to assess two potential limiting factors of the manoeuvring performance of hummingbirds: (1) muscle mechanical power output and (2) delays in the neural sensing and control system. We focused on the magnificent hummingbird (*Eugenes fulgens*, 7.8 g) and the black-chinned hummingbird (*Archilochus alexandri*, 3.1 g), which represent large and small species, respectively. We first estimated the aerodynamic forces, moments and the mechanical power of escape manoeuvres using measured wing kinematics. Comparing active-manoeuvring and passive-damping aerodynamic moments, we found that pitch dynamics were lightly damped and dominated by the effect of inertia, while roll dynamics were highly damped. To achieve observed closed-loop performance, pitch manoeuvres required faster sensorimotor transduction, as hummingbirds can only tolerate half the delay allowed in roll manoeuvres. Accordingly, our results suggested that pitch control may require a more sophisticated control strategy, such as those based on prediction. For the magnificent hummingbird, we estimated that escape manoeuvres required muscle mass-specific power 4.5 times that during hovering. Therefore, in addition to the limitation imposed by sensorimotor delays, muscle power could also limit the performance of escape manoeuvres.

KEY WORDS: Neural delay, Dynamics, Scaling, Muscle, Aerodynamics, Power

INTRODUCTION

As the 'vertebrate analogue' of flying insects, hummingbirds have achieved unparalleled manoeuvrability, particularly at slow flight speed and in confined space. For these miniature vertebrate fliers, mastering a repertoire of controlled aerobatic manoeuvres is essential for their aerial survival (Altshuler, 2006; Clark, 2011; Sholtis et al., 2015) and sexual selection (Clark, 2009; Clark et al., 2011; Stiles, 1982). In a companion paper (Cheng et al., 2016), we studied the kinematic patterns of one such manoeuvre, an escape response consisting of drastic body pitch and roll rotations combined with large unidirectional linear acceleration. Following this kinematic analysis, here we further assess the manoeuvrability of hummingbirds using a system- and control-theoretic perspective, to understand the underlying limiting factors of flight performance.

For flying animals, the primary limiting factors of flight performance or manoeuvrability are arguably twofold: (1) attainable muscle mechanical power output (Altshuler et al., 2010a; Ellington, 1985 1991; Marden, 1994) associated with generation of aerodynamic manoeuvring forces and moments that create and maintain fast body movements, and (2) effective coordination of these movements using fast and accurate flight-sensing and motor-control systems (Altshuler et al., 2012, 2010b; Goller and Altshuler, 2014; Iwaniuk and Wylie, 2007; Warrick et al., 2002). Limits of muscle mechanical power of hummingbirds have been extensively tested using load-lifting performance in short-burst flight (Altshuler et al., 2010a; Chai et al., 1997; Chai and Dudley, 1995; Marden, 1987, 1994). It has been argued that the limits may derive from physiological constraints in muscle contractile force and speed, anatomical constraints of wing motion or aerodynamic constraints (Altshuler et al., 2010a; Ellington, 1991). For the majority of these studies (Chai and Millard, 1997; Dickinson et al., 1998; Fry et al., 2005), muscle-specific power has been estimated using a simplified aerodynamic model derived from the work of Ellington (1984), which substantially underestimates power according to modern analyses based on more accurate estimation of aerodynamic forces (Song et al., 2014b; Sun and Tang, 2002).

Coordination of body and wing movements in rapid flight manoeuvres also demands sensorimotor transduction that computes and enforces flight-control algorithms with desired computation complexity and speed (Beatus et al., 2015; Fuller et al., 2014; Ristroph et al., 2013; Roth et al., 2012). For fruit flies (*Drosophila*), large sensorimotor delay prevents their mechanosensory organs from stabilizing unstable flight dynamics (Chang and Wang, 2014; Cheng et al., 2011; Elzinga et al., 2012) and results in unstable oscillation of ground-speed regulation under high-gain visual feedback (Fuller et al., 2014). A recent study suggests that limiting effects of sensorimotor delays in prey interception of dragonflies can be partially mediated by employing more sophisticated internal models in the flight controller (Mischiati et al., 2015), which are commonly found in vertebrate locomotion control (Flanagan and Wing, 1997; Wolpert and Ghahramani,

[1]Department of Mechanical and Nuclear Engineering, Pennsylvania State University, University Park, PA 16802, USA. [2]Field Research Station at Fort Missoula, Division of Biological Sciences, University of Montana, Missoula, MT 59812, USA. [3]Biology & Chemistry Department, George Fox University, Newberg, OR 97132, USA. [4]Department of Biology, University of North Carolina, Chapel Hill, NC 27599, USA. [5]School of Mechanical Engineering, Purdue University, West Lafayette, IN 47907, USA. [6]Hummingbird Monitoring Network, PO Box 115, Patagonia, AZ 85624, USA.

*Author for correspondence (buc10@psu.edu)

B.C., 0000-0002-6982-0811

Received 18 January 2016; Accepted 23 August 2016

Journal of Experimental Biology

Journal of Experimental Biology (2016) 219, 3532-3543 doi:10.1242/jeb.137570

List of symbols and abbreviations

b	damping coefficient with respect to an axis of rotation
CFD	computational fluid dynamics
$C(s)$	transfer function of the neural controller
$\mathbf{F}$	total aerodynamic force
$\mathbf{F}_{add}$	added mass component of the normal force
$\mathbf{F}_{D,trans}$	translational component of drag force
$\mathbf{F}_{L,trans}$	translational component of lift force
$\mathbf{F}_{rot}$	rotational component of the normal force
$H(s)$	transfer function of the sensing and motor delays
I	moment of inertia about an axis of rotation
K	controller gain
K_I	integral controller gain
K_P	proportional controller gain
m	body mass
m_{muscle}	flight muscle mass
MOI	moment of inertia
n	wingbeat frequency
P_{aero}	aerodynamic power
PD	proportional-derivative (controller)
PI	proportional-integral (controller)
P^*_{hover}	muscle mass-specific power during hover
P^*_{pitch}	muscle mass-specific power during pitch
P^*_{roll}	muscle mass-specific power during roll
$P(s)$	transfer function of the open-loop dynamics
R	wing length
$\hat{r}$	dimensionless spanwise location
s	complex frequency
T	single-axis aerodynamic moment
T_m	aerodynamic moment produced by the nominal manoeuvring wing kinematic pattern
$\mathbf{T}_{total}$	total aerodynamic moment
$\mathbf{v}$	local linear velocity of a blade element
$\mathbf{v}_h$	wing hinge velocity
(x_w, y_w, z_w)	wing coordinate frame
α	angle of attack
γ_L	an indicator of the magnitude of wing kinematic change during roll
γ_M	an indicator of the magnitude of wing kinematic change during pitch
Δt	lumped delay in the neural sensing and motor control system
θ	angular position of an axis of rotation
θ_r	reference angular position of an axis of rotation
τ_a	active manoeuvring time constant
τ_c	controller time constant
τ_{CL}	closed-loop time constant
τ_p	open-loop time constant
Φ	wingbeat amplitude
$\boldsymbol{\omega}$	local angular velocity of a blade element
$\boldsymbol{\omega}_b$	body angular velocity
ω_m	maximum stroke-averaged angular rate of the manoeuvre
$\boldsymbol{\omega}_w$	wing angular velocity relative to the body frame

2000). A rigorous analysis of insect sensorimotor flight control can be derived from parsimonious modelling of the physics of flight (or mechanical models, Miller et al., 2012) and neural sensing and motor systems in the framework of classical feedback control theory (Cowan et al., 2014; Franklin et al., 1994). This approach has received increasing attention recently, applied to pitching manoeuvres of hawkmoths (Cheng et al., 2011), flight stabilization of fruit flies under perturbations that induce roll (Beatus et al., 2015), pitch (Ristroph et al., 2013) and yaw (Ristroph et al., 2010), and ground-speed regulation using visual and mechanosensory feedbacks (Fuller et al., 2014).

In this paper, we extend the kinematic analysis of our companion paper (Cheng et al., 2016) to assess how flight performance of hummingbird escape manoeuvres is related to mechanical power output of their muscles and to delays in their neural sensing and motor-control systems. Escape manoeuvres from vigilant hummingbirds under potential threat may represent a near-maximal flight performance, thereby revealing effects of underlying limiting factors. We first calculate aerodynamic forces, moments and mechanical power of escape manoeuvres using measured wing kinematics and quasi-steady aerodynamic modelling. At high angular rates of change in body orientation, animals with flapping wings may experience substantial damping as a result of asymmetries of wing motion caused by body rotation; this is known as flapping counter torque (Hedrick et al., 2009). Thus, we estimate damping and the corresponding time constant of averaged open-loop dynamics to quantify the relative importance of damping and inertia. We then assess potential performance limitations imposed by delays in neural sensing and control systems and by muscle power. Finally, we explore interspecific differences in muscle power and their implications for flight performance. For clarity and concision, among the four species studied in the companion paper, we focus only on magnificent hummingbirds and black-chinned hummingbirds, representing large and small species, respectively.

MATERIALS AND METHODS

Aerodynamic model of flapping wings

We estimate aerodynamic forces and moments produced by flapping wings using blade-element analysis (Leishman, 2006) and quasi-steady aerodynamic models (Sane and Dickinson, 2002). Our method extends the previous methods by introducing spanwise twist and incorporating body velocities.

We first divide a wing into blade elements whose spanwise distances from the shoulder are specified by $\hat{r}$. Because of wing spanwise twist, local blade angular and linear velocities, $\boldsymbol{\omega}$ and $\mathbf{v}$, respectively, and angle of attack, α, vary with time t and $\hat{r}$, and are calculated as:

$$\boldsymbol{\omega}(\hat{r},t) = \boldsymbol{\omega}_w(\hat{r},t) + \boldsymbol{\omega}_b(t), \quad (1)$$

$$\mathbf{v}(\hat{r},t) = \boldsymbol{\omega} \times R\hat{r}\hat{\mathbf{y}}_w + \mathbf{v}_h(t), \quad (2)$$

$$\alpha(\hat{r},t) = |\mathrm{atan2}(\mathbf{v}_{xz} \cdot \hat{\mathbf{x}}_w, \mathbf{v}_{xz} \cdot \hat{\mathbf{z}}_w)|, \quad (3)$$

where $\boldsymbol{\omega}_w(\hat{r},t)$ is angular velocity of the wing relative to the body, obtained using derivatives of wing Euler angles, $\phi(t)$, $\theta(t)$ and $\psi(t,\hat{r})$ (see the kinematic model of flapping wings in Cheng et al., 2016); $\boldsymbol{\omega}_b(t)$ is angular velocity of the body; $\mathbf{v}_h(t)=\mathbf{v}_b(t)+\boldsymbol{\omega}_b(t)\times\mathbf{l}_h$ is linear velocity at the wing base due to body rotation and translation, where $\mathbf{v}_b(t)$ is linear velocity of the body and $\mathbf{l}_h$ is a position vector from the centre of mass to the wing base; R is wing length; $\mathbf{v}_{xz} = \mathbf{v}_{xz}(\hat{r},t)$ is local blade velocity projected on the transverse X–Z plane of a wing blade element (i.e. excluding the long-axis y-component); and $[\hat{\mathbf{x}}_w(\hat{r},t), \hat{\mathbf{y}}_w(t), \hat{\mathbf{z}}_w(\hat{r},t)]$ are axes of the local blade-element coordinate frame. As a result of wing twist, $\hat{\mathbf{x}}_w$ and $\hat{\mathbf{y}}_w$ are also functions of $\hat{r}$.

At each blade element, the local aerodynamic force vector ($d\mathbf{F}$, Eqn 4) is the sum of force components due to three distinct aerodynamic mechanisms: (1) wing translational forces due to delayed stall ($d\mathbf{F}_{L,trans}$ and $d\mathbf{F}_{D,trans}$, Eqns 5 and 6) (Dickinson et al., 1999), (2) rotational lift ($d\mathbf{F}_{rot}$, Eqn 7) (Sane and Dickinson, 2002)

and (3) added mass ($d\mathbf{F}_{add}$, Eqn 8) (Sedov, 1965; Whitney and Wood, 2010):

$$d\mathbf{F} = d\mathbf{F}_{L,trans} + d\mathbf{F}_{D,trans} + d\mathbf{F}_{rot} + d\mathbf{F}_{add}, \quad (4)$$

$$d\mathbf{F}_{L,trans}(\hat{r},t) = q\, C_L(\alpha)\, \hat{\mathbf{e}}_L c(\hat{r}) R d\hat{r}, \quad (5)$$

$$d\mathbf{F}_{D,trans}(\hat{r},t) = q\, C_D(\alpha) \hat{\mathbf{e}}_D c(\hat{r}) R d\hat{r}, \quad (6)$$

$$d\mathbf{F}_{rot}(\hat{r},t) = \rho\pi(0.25 - \hat{c}_r)\omega_y c(\hat{r})^2 R |\mathbf{v}_{xz}| \hat{\mathbf{x}}_w d\hat{r}, \quad (7)$$

$$d\mathbf{F}_{add}(\hat{r},t) = (-\lambda_x \dot{v}_x - \lambda_{x\omega}\dot{\omega}_y) R \hat{\mathbf{x}}_w d\hat{r}, \quad (8)$$

where $c(\hat{r})$ is local chord length; $q = q(\hat{r},t) = \frac{1}{2}\rho|\mathbf{v}_{xz}(\hat{r},t)|^2$ is local instantaneous dynamic pressure; $\hat{\mathbf{e}}_L = \mathbf{R}_y\left(-\frac{v_x}{|v_x|}\frac{\pi}{2}\right)\hat{\mathbf{v}}_{xz}$ and $\hat{\mathbf{e}}_D = -\hat{\mathbf{v}}_{xz}$ are unit directional vectors of lift and drag forces, respectively; and $C_L(\alpha)$ and $C_D(\alpha)$ are local instantaneous lift and drag coefficients, respectively, which are functions of α. Functions of C_L and C_D have been obtained in previous works using theoretical modelling (Nabawy and Crowther, 2014; Taha et al., 2014), regressions to experimental data (Dickinson et al., 1999; Lentink and Dickinson, 2009; Usherwood and Ellington, 2002) and computational fluid dynamic (CFD) simulation (Song et al., 2014a; Wang et al., 2004). We used results reported in recent CFD flow simulation of the ruby-throated hummingbird (*Archilochus colubris*) (Song et al., 2014a), i.e. C_L=0.245+1.63sin(2.34α–6.30) and C_D=1.88–1.70cos(2.27α–10.66), where α is in degrees. Note that the hummingbird species we studied have Reynolds numbers between 8500 and 13,000, a range over which force coefficients have negligible variation (it has been shown that force coefficients change quite little for Reynolds numbers from the order 10^2 to 10^5; Lentink and Dickinson, 2009). $\hat{c}_r = c_r(\hat{r})/c(\hat{r})$ is the normalized distance between the axis of wing rotation (or wing pitch) and the mid-point of wing chord ($-0.5 \le \hat{c}_r \le 0.5$), and coefficients of virtual mass λ_x=$\pi\rho[0.5c(r)]^2$ and $\lambda_{x\omega}$=–$\pi\rho[0.5c(r)]^2 c_r$ are derived using potential flow theory (Sedov, 1965).

Next, the resultant moment vector about the base of the wing from each blade element is calculated:

$$d\mathbf{T}_{total} = \mathbf{r}_{trans} \times (d\mathbf{F}_{L,trans} + d\mathbf{F}_{D,trans}) + \mathbf{r}_{rot} \times d\mathbf{F}_{rot} + \mathbf{r}_{add} \times d\mathbf{F}_{add}, \quad (9)$$

where $\mathbf{r}_{trans}$, $\mathbf{r}_{add}$ and $\mathbf{r}_{rot}$ are moment arms for each force component (Dickson et al., 2006):

$$\mathbf{r}_{trans} = \hat{r}R\hat{\mathbf{y}}_w - c(r)\left[0.82\frac{|\alpha|}{\pi} + 0.05\right]\hat{\mathbf{z}}_w, \quad (10)$$

$$\mathbf{r}_{add} = \mathbf{r}_{rot} = \hat{r}R\hat{\mathbf{y}}_w. \quad (11)$$

Here we neglected the moment about wing spanwise axis ($\hat{\mathbf{y}}_w$) due to added mass and rotational lift as the aerodynamic moment was dominated by the chordwise component and the aerodynamic force was dominated by the translational component. The aerodynamic power produced by each wing blade is computed as the dot-product of the force and velocity vectors:

$$dP_{aero}(\hat{r},t) = -d\mathbf{F}(\hat{r},t) \cdot \mathbf{v}(\hat{r},t). \quad (12)$$

Finally, the total aerodynamic forces, moments and aerodynamic power of the wing are obtained by the summation of the respective quantities from all blade elements. The aerodynamic power estimated here can be used to predict muscle-mechanical power output. By assuming perfect or zero muscle elastic energy storage, we can obtain the minimum or maximum estimates of the required muscle mass-specific power (Chai and Millard, 1997; Ellington, 1984). Herein, we only consider minimum estimates as they reveal minimum power requirements for achieving observed flight performance.

Calculation of forces, moments, power and passive-damping coefficients

We apply the above aerodynamic model to calculate forces and moments produced by hovering and manoeuvring wing kinematics (Cheng et al., 2016), first assuming the body was stationary. To calculate the aerodynamic power associated with the manoeuvring wing kinematics, we included the effects of body motion by adding constant linear and angular velocities estimated using stroke-averaged body velocities to wing velocity. This is crucial because body motion changes the effective wing velocities and angles of attack and is expected to reduce aerodynamic power. The aerodynamic power associated with pitch and roll manoeuvring wing kinematics is then calculated individually (P_{pitch} and P_{roll}).

We estimate the passive damping coefficient of body rotation using a varying angular rate about the axis of rotation and calculating the resultant counter-moments based on our aerodynamic model. To do this, we vary incrementally over 20 steps the components of angular velocity from −1500 to −1500 deg s^{-1}, and then calculate the resulting moment. Passive damping coefficients are then obtained by regressing of stroke-averaged moments as a function of angular rate (Cheng et al., 2011).

Modelling of rotational flight dynamics

We derive a simplified single-degree-of-freedom rotational-dynamic model and related time constants, which will be used to analyze the flight dynamics and control of the escape manoeuvres. Note that while performing a rotational manoeuvre, a hummingbird produces aerodynamic moments using active changes of wing motion to overcome both the damping and inertia moments (Cheng et al., 2010; Fry et al., 2003; Muijres et al., 2015). Neglecting aerodynamic and inertia coupling terms, the flight dynamics can be simplified into the following equation of motion:

$$I\ddot{\theta}(t) + b\dot{\theta}(t) = T(t), \quad (13)$$

where I and b are body moment of inertia and damping coefficient, respectively, with respect to the rotational axis (for estimation of body moments of inertia, see the Appendix), $\dot{\theta}$ and $\ddot{\theta}$ are angular velocity and acceleration, respectively, and T is the aerodynamic moment.

Based on Eqn 13, it can be seen that the flight dynamics could be either dominated by the damping ($b\dot{\theta}$) or the inertia ($I\ddot{\theta}$), depending on their relative magnitudes. The relative dominance of damping and inertia depends crucially on the pertinent open-loop dynamics (e.g. pitch or roll) and varies with the types of manoeuvres. To facilitate quantitative analysis, we can make use of the following time constants (without discerning pitch and roll). The open-loop time constant is calculated as:

$$\tau_p = I/b, \quad (14)$$

and represents the intrinsic time scale of the open-loop dynamics without control.

The active-manoeuvring time constant is calculated as:

$$\tau_a = \frac{\omega_m(1 - e^{-1})}{T_m/I}, \quad (15)$$

Journal of Experimental Biology (2016) 219, 3532-3543 doi:10.1242/jeb.137570

Table 1. Acceleration and time constants pertinent to pitch dynamics and control

	$\bar{\dot{q}}$ (deg ms^{-2})	q_{cycle} (deg ms^{-1})	$\bar{q}_m$	τ_p (ms) (wingbeat)	τ_a (ms) (wingbeat)	τ_{CL} (ms) (wingbeat)
Magnificent hummingbird (*Eugenes fulgens*)	0.128	3.51	1.843	69.7 (2.54)	9.1 (0.33)	33.6 (1.22)
Black-chinned hummingbird (*Archilochus alexandri*)	0.053	0.90	1.550	191.9 (11.31)	18.6 (1.10)	48.0 (2.84)

Quantities include: maximum pitch acceleration ($\bar{\dot{q}}$) and increase of the angular velocity the birds are able to achieve within one wing stroke (q_{cycle}); both are calculated using nominal wing kinematics during pitch, maximum stroke-averaged roll rate of the manoeuvre ($\bar{q}_m$), open-loop time constants of pitch dynamics (τ_p), active-manoeuvring time constant (τ_a) and observed closed-loop time constants (τ_{CL}). Numbers in parentheses are wingbeat time normalized by the wingbeat period.

where ω_m is the maximum stroke-averaged angular rate of the manoeuvre (Tables 1, 2) and T_m is the aerodynamic moment produced by the nominal manoeuvring wing kinematic pattern obtained from the pitching or rolling phase of the escape manoeuvre. This time constant is seen as the counterpart of τ_p, as it represents the time spent to accelerate the inertia to 63% of the maximum velocity assuming no damping. This quantifies the time scale associated with the active effort for manoeuvring.

A third quantity, the closed-loop time constant, can be calculated as:

$$\tau_{CL} = t_{63\%}, \tag{16}$$

and characterizes the speed of the closed-loop flight system. If we assume that the desired angular velocity profile can be approximated by a rectangular pulse function and the angular position by a ramp function, τ_{CL} will be equivalent to the actual time spent to reach 63% of the maximum angular velocity, which can be obtained from observed body kinematics.

Modelling of flight control

We introduce a hypothetical flight control model of the escape manoeuvres, and then based on this model, we derive the fastest closed-loop response achievable, as measured by the lowest closed-loop time constant τ^*_{CL}. For both pitch and roll manoeuvres, as suggested by a number of previous studies (Beatus et al., 2015; Cheng et al., 2011; Ristroph et al., 2010), we first assume that the functional principles of the underlying neural sensing and motor control system can be modelled parsimoniously using a proportional-integral (PI) controller that depends on the sensory feedback of angular rate. A PI controller, or an equivalent proportional-derivative (PD) controller, assuming the angle is measured directly, also captures the feedback control principle of cockroach wall following Cowan et al. (2006). We assume that associated delays in neural sensing and motor control are lumped into a single delay (Δt) in the control loop (Fig. 1). To perform a rotational manoeuvre, the desired angular rate and position provided by the central nervous system are compared with the delayed measurements of angular rate and position, and the aerodynamic moment is generated proportional to the difference:

$$T(t) = -K_I[\theta(t-\Delta t) - \theta_r(t)] - K_P[\dot{\theta}(t-\Delta t) - \dot{\theta}_r(t)]. \tag{17}$$

Next, through the Laplace transform, overall closed-loop flight dynamics are represented by transfer functions in the frequency domain, a common representation used in control theory (Franklin et al., 1994):

$$C(s) = K(1+\tau_c s), \tag{18}$$

$$H(s) = e^{-\Delta t s}, \tag{19}$$

$$P(s) = \frac{1/I}{\left(s+\frac{1}{\tau_p}\right)}, \tag{20}$$

where $C(s)$, $H(s)$ and $P(s)$ represent transfer functions of neural controller, sensing and motor delays, and open-loop dynamics, respectively; s is complex frequency; and τ_c and K are defined as controller time constant and gain (K=K_I and K_P=$K\tau_c$). In classical control theory, closed-loop stability and performance of the system depend primarily on the roots of the characteristic equation of the system:

$$1 + C(s)H(s)P(s)/s = 0. \tag{21}$$

The closed-loop time constant τ_{CL} can be estimated according to the dominant root of Eqn 21 (the root that has largest real component). The time delay is first represented by a third-order rational function using Padé approximation (Franklin et al., 1994), and the roots for each combination of τ_c and Δt are found by plotting the root locus of Eqn 21 for gain K_P from 0 to ∞ in MATLAB (MathWorks, Natick, MA, USA). For a hummingbird of given open-loop time constant τ_p and moment of inertia I, this allows us to assess the dependence of τ_{CL} on the coefficients K_P and τ_c in the neural controller and the lumped delay Δt. Assuming hummingbirds have exploited the 'best' neural controller by selecting the K^* and τ^*_c that result in the lowest τ^*_{CL} (or the fastest response achievable), we derive the performance limitation of the manoeuvre as a function of the delay Δt:

$$\tau^*_{CL}(\Delta t) = \tau^*_{CL}(\Delta t, K^*, \tau^*_c) = 1/\max_{K,\tau_c}|Re(p_d)|$$
$$= 1/\max_{K,\tau_c}[\min_i |Re(p_i)|], \tag{22}$$

where p_i and p_d represent the roots and the dominant root of Eqn 21, i is from 1 to N (N=4 is the order of the equation), and $Re()$ represents the real part of the complex number.

Table 2. Acceleration and time constants pertinent to roll dynamics and control

	$\bar{\dot{p}}$ (deg ms^{-2})	p_{cycle} (deg ms^{-1})	$\bar{p}_m$	τ_p (ms) (wingbeat)	τ_a (ms) (wingbeat)	τ_{CL} (ms) (wingbeat)
Magnificent hummingbird (*Eugenes fulgens*)	0.095 0.266*	2.567	1.852	10.9 (0.40)	12.3 (0.46) 4.38* (0.16*)	38.1
Black-chinned hummingbird (*Archilochus alexandri*)	0.040 0.103*	0.750	2.275	20.7 (1.10)	36.0 (1.92) 13.97* (0.75*)	41.0

Definitions are as in Table 1, but for roll.
*Quantities calculated based on averages over downstroke instead of a complete stroke cycle.

Journal of Experimental Biology (2016) 219, 3532-3543 doi:10.1242/jeb.137570

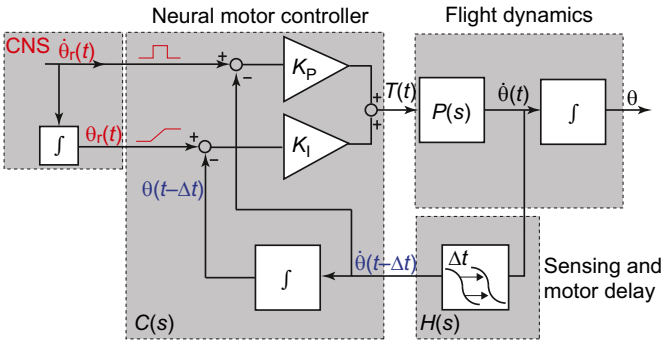

Fig. 1. Hypothesized closed-loop rotational flight dynamics of hummingbirds using the most parsimonious block diagram. Without specifying the specific biological sensory organs (vision or proprioception), it is assumed that body angular velocity $\dot{\theta}$ is measured directly by the hummingbirds. Latencies in neural sensing and motor control systems have been lumped into a single delay Δt in the feedback loop. The desired angular rate $\dot{\theta}_r$ and position θ_r instructed by the central nervous system (CNS) are compared with measured angular rate and integrated position, both of which are delayed by Δt. Resulting velocity and position errors are used by the neuromuscular controller, through proportional and integral control actions, to generate flight control moment T that rotates the body of the hummingbird. Desired angular velocity is assumed as a rectangular pulse function and desired angular position as a ramp function. $C(s)$, $H(s)$ and $P(s)$ are transfer functions of neural controller, sensing and motor delays, and open-loop dynamics, respectively. K_I, integral controller gain; K_P, proportional controller gain.

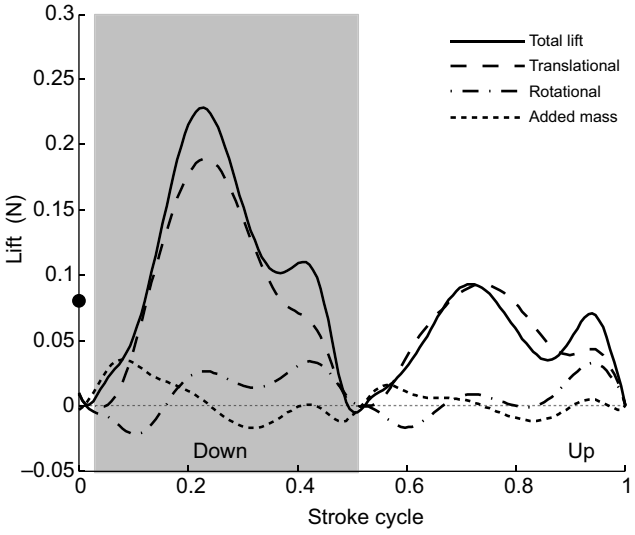

Fig. 2. Lift force of magnificent hummingbirds calculated using quasi-steady aerodynamic modelling. Individual components due to different aerodynamic mechanisms include the translational component (Eqn 5), rotational lift (Eqn 7) and added mass (Eqn 8). Shading indicates downstroke. Stroke-averaged total lift is the solid circle on the ordinate.

RESULTS

Aerodynamic forces and power in hovering

Our calculations showed that a hovering downstroke generated more than twice the lift of an upstroke (two times for magnificent hummingbirds and 2.7 times for black-chinned hummingbirds), consistent with previous studies (Song et al., 2014b; Warrick et al., 2005). We attribute this disparity between half strokes to spanwise twist of the wing, which was greater during upstroke (Cheng et al., 2016). Examining lift components due to different aerodynamic mechanisms showed that the forces were dominated by the 'steady' translational component, while unsteady components (i.e. added mass and rotational lift) only augmented the lift by a small amount (Fig. 2).

Both species generated roll and pitch moments in a similar manner. For example, roll moment was generated mainly during downstroke (Fig. 3); pitch-up moment was generated when the wing was ventral to the body, and, conversely, pitch-down moment was generated when the wing was dorsal; pitch moment was mainly based on lift instead of drag.

Stroke-averaged muscle mass-specific power (P^*_{hover}) was 185 W kg^{-1} in magnificent hummingbirds and 227.8 W kg^{-1} in black-chinned hummingbirds. Both estimates were much higher than those predicted using Ellington's model (e.g. 76 W kg^{-1} for the magnificent hummingbird and 87 W kg^{-1} for the black-chinned hummingbird; Chai and Millard, 1997), but similar to the 190 W kg^{-1} predicted for ruby-throated hummingbirds using high-fidelity CFD (Song et al., 2014b).

Aerodynamic forces and moments in escape manoeuvres

During active manoeuvring, the aerodynamic forces, moments and muscle mechanical power output of the wings depend on three factors: (1) the active change of wing kinematics from hovering, (2) increases of flapping frequency and (3) body linear and angular velocities. The former two create active manoeuvring forces and moments to overcome passive damping due to body velocities and accelerate body inertia. In this section, we first analyze in detail the patterns of manoeuvring forces and moments generated during the pitching and rolling phases of the escape manoeuvre. In the next section, we investigate passive damping due to body rotations. These results are then used to assess the overall flight dynamics, control and performance limitations in the Discussion.

Forces and moments calculated using nominal manoeuvring wing kinematics were qualitatively similar in both species; so we focus our description on magnificent hummingbirds exhibiting pitch (Fig. 4A–C) and roll (Fig. 4D–F). Substantial pitch-up moment (Fig. 4C) was created during the entire downstroke, while that during upstroke remained unchanged, and its peak value was almost five times that of hovering flight (dashed curves). In contrast with the lift-based pitch moment in hovering flight, in manoeuvring flight the pitch moment was modulated primarily by the augmented rearward drag force created during the downstroke (Fig. 4A), while there was a relatively small change in the forward force during the upstroke. The drastic increase of rearward drag force also confirmed that the hummingbirds were able to significantly change the direction of aerodynamic forces (e.g. tilt the force vector rearward; Cheng et al., 2016), and therefore do not conform to the 'helicopter model', which was found previously to be valid for escape manoeuvres in fruit flies (Muijres et al., 2014). The results also show that the magnitude of the total aerodynamic force (combining the averaged lift and fore/aft forces in Fig. 4A,B) is approximately doubled during the pitching phase, which is comparable to those in escaping fruit flies. Unlike the pitch moment, both positive and negative roll moments were created within a stroke cycle, while downstroke was responsible for creating most of the positive 'steering' roll moment and upstroke created a smaller amount of 'braking' negative roll moment (red curve, Fig. 4D).

Stroke-averaged values of pitch and roll manoeuvring moments, which corresponded to the wingbeat cycle of the maximum change of wing kinematics (Cheng et al., 2016), can be used to estimate the maximum angular acceleration and the increase of the angular velocity the birds were able to gain within one wing stroke (Tables 1, 2). Average pitch moments were 4.72 N mm (or $0.83mgR$, where m is body mass, g is gravitational acceleration

Journal of Experimental Biology (2016) 219, 3532-3543 doi:10.1242/jeb.137570

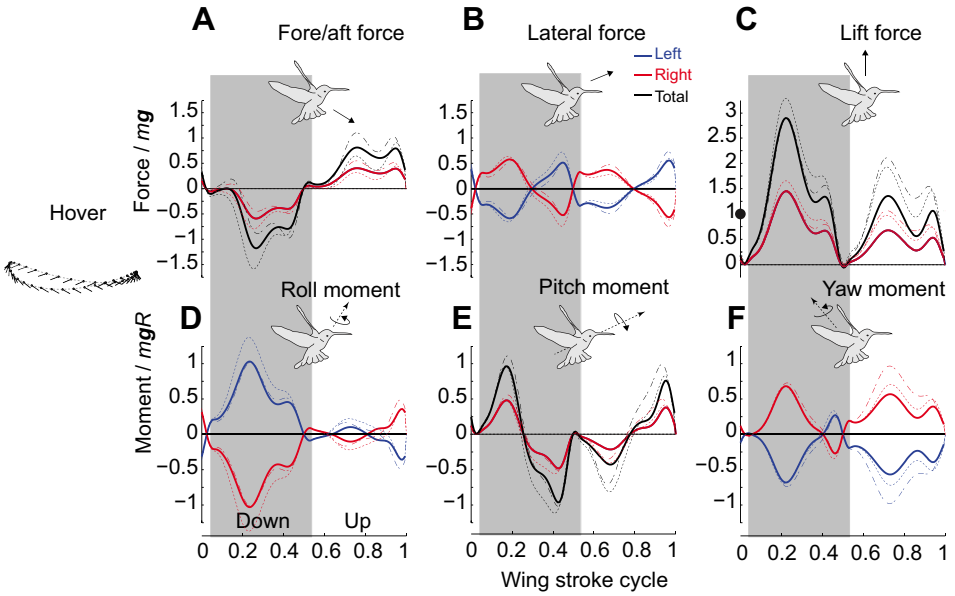

Fig. 3. Instantaneous aerodynamic forces and moments of magnificent hummingbirds during hovering. (A) Fore/aft force, (B) lateral force, (C) lift force, (D) roll moment, (E) pitch moment and (F) yaw moment calculated using the nominal hovering wing kinematic pattern (moments are about principal axes of body). Forces are normalized to body weight (*mg*) and moments are normalized to body weight and wing length (*mgR*). Red and blue curves indicate left and right wing quantities (if identical, only those of right wing are shown), and total force and moments are solid black. Averaged lift (equals body weight) is the solid circle on the ordinate in C. Dash-dotted and dotted curves show forces and moments calculated based on the nominal wing kinematics ±s.d., respectively. Note that because of aerodynamic nonlinearities, these do not bracket the nominal kinematic result.

and R is wing length) and 0.44 N mm (0.31*mgR*) for magnificent and black-chinned hummingbirds, respectively. These yielded angular accelerations of 0.128 and 0.0527 deg ms^{-2} (Table 1) and increases in angular velocity up to 3506 and 895 deg s^{-1} in a single wingbeat cycle. Thus the larger magnificent hummingbirds performed much faster pitch manoeuvres than the smaller black-chinned hummingbirds, and, without damping, they would have reached peak pitch rate using only approximately one wing stroke. Average roll moments created were 1.59 N mm (0.28*mgR*) and 0.13 N mm (0.092*mgR*) for magnificent and black-chinned hummingbirds, respectively, which yielded angular accelerations of 0.095 and 0.040° ms^{-2}, and led to increases in roll velocity of up to 2567 and 750 deg s^{-1} in a single wingbeat cycle (Table 2).

Aerodynamic damping during body rotations

For magnificent hummingbirds, the damping coefficient of pitch rotation was 0.53×10^{-3} N mm deg^{-1} s, corresponding to a damping moment of 1.16 N mm (0.20*mgR*) at the maximum pitch rate observed, and was approximately 25% of the magnitude of the active manoeuvring moment estimated (4.72 N mm or 0.83*mgR*). The damping coefficient of roll rotation was 1.53×10^{-3} N mm deg^{-1} s, which corresponded to a damping moment of 2.86 N mm (0.49*mgR*) at the maximum roll rate. Thus, the damping moment was higher than the manoeuvring roll moment because of active modulation of wing kinematics (1.59 N mm, or 0.28*mgR*). Thus, damping was more significant in roll dynamics than in pitch dynamics.

The hummingbirds always flared their tails during the manoeuvres, and their flared tails were similar in surface area to that of a single wing (Cheng et al., 2016). However, numerical simulation of wingless body-and-tail models of hummingbirds indicated that damping from the tail was relatively small compared with that from the wings, so in subsequent analyses we neglect tail contributions. For roll and yaw, damping from the tail was two

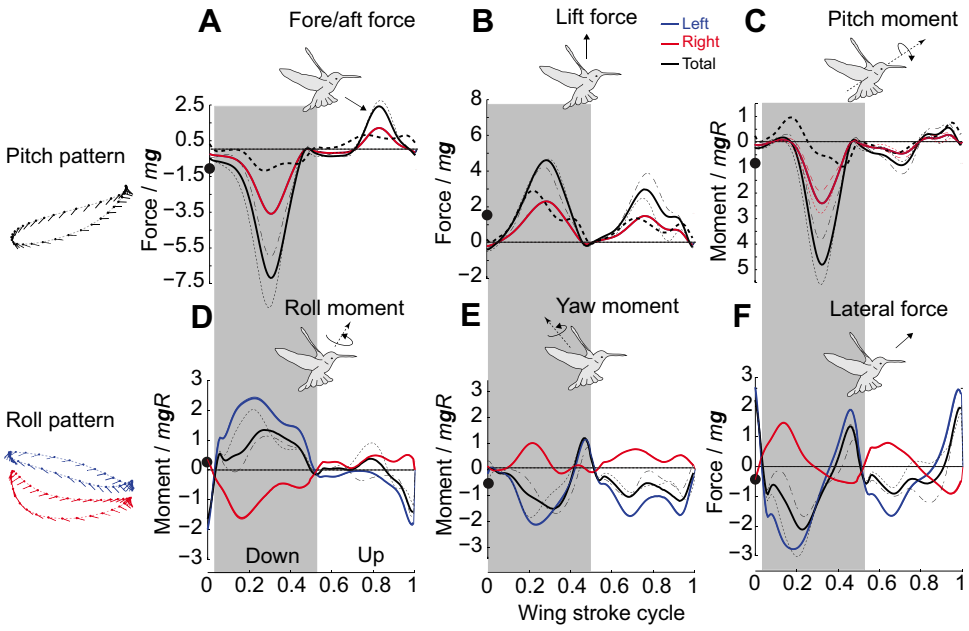

Fig. 4. Instantaneous aerodynamic forces and moments of manoeuvring magnificent hummingbird. (A) Force/aft force, (B) lift force and (C) pitch moment calculated using the nominal pitch manoeuvring pattern, (D) roll moment, (E) yaw moment and (F) lateral force calculated based on the nominal roll manoeuvring pattern (all the moments are about body principal axes). Forces are normalized by *mg* and moments are normalized by *mgR*. Colour curves are defined same as those in Fig. 3. Hovering forces and moments (dashed black curves) are plotted for reference. Average manoeuvring forces and moments are filled circles on the ordinates. Dash-dotted and dotted curves show the forces and moments calculated based on the nominal wing kinematics ±s.d., respectively. A complete set of force and moments plots is shown in Fig. S1.

Journal of Experimental Biology (2016) 219, 3532-3543 doi:10.1242/jeb.137570

orders of magnitude lower than that from the wings. For pitch, although it was found that the tail increased the damping by approximately 20%, its effect was negligible because pitch dynamics were lightly damped, and the damping moment from the wings was significantly lower than the active manoeuvring moment. Thus, we estimate that a 20% increase in pitch damping had a negligible (<5%) effect on the pitch dynamics (using results from magnificent hummingbirds). This is consistent with the observation from Clark (2011) that the tail does not have a significant effect on the flight performance of low-speed manoeuvres.

Aerodynamic power in escape manoeuvres

Muscle mass-specific power expenditure for manoeuvring was significantly different between the two species (Table 3). Although the smaller black-chinned hummingbirds required more mass-specific power to hover than larger magnificent hummingbirds, they used less power during the escape manoeuvres, and both species achieved similar rolling rates. For example, magnificent hummingbirds, with an increase of wingbeat frequency of approximately 50% during the manoeuvre, required a muscle mass-specific power of 590 W kg^{-1} during the pitching phase (with upper and lower bounds estimated at 500 and 772 W kg^{-1} using nominal manoeuvring kinematics ±s.d.; Cheng et al., 2016), compared with 185 W kg^{-1} in hovering flight. Black-chinned hummingbirds, in contrast, output 482 W kg^{-1}, compared with 228 W kg^{-1} during hovering. More remarkably, magnificent hummingbirds required as much as 881 W kg^{-1} for the outer (steering) wing in the second half of the manoeuvre when rolling at their maximum rate. Black-chinned hummingbirds, which showed a smaller increase in wingbeat frequency, used less power (361 W kg^{-1}) to roll at similar rates compared with magnificent hummingbirds.

Effects of uncertainties in wing kinematics

Wing kinematics exhibit variance, including biological variation and measurement error, both of which are included in the standard deviations of wing angles in hovering and manoeuvring kinematics (Cheng et al., 2016). This variance propagates through the aerodynamic model and leads to variations in estimated forces and moments. However, this process is extremely nonlinear owing to the complexity of the aerodynamic model. We confirmed this complexity by calculating the hovering and maneuvering forces, moments and power using corresponding nominal wing kinematics and their standard deviations. For example, in Figs 3 and 4, the absolute values of peak forces and moments bracketed using ±s.d. were sometimes greater than the absolute values of the nominal peak. However, variations in the forces and moments owing to variance in wing kinematics did not affect the general trends emerging from modelling nominal wing kinematics. Therefore, our subsequent discussion is developed using only the results from nominal wing kinematics.

DISCUSSION

Damping versus inertia in flight dynamics

The relative dominance of damping and inertia terms has profound implications on neuromuscular control and neurosensory feedback of manoeuvres (Hedrick et al., 2009; Hesselberg and Lehmann, 2007; Reichardt and Poggio, 1976; Springthorpe et al., 2012). For example, if flight dynamics were dominated by inertia, to achieve desired manoeuvring performance, an animal would need to rely on fast sensory feedback and neuromuscular control that actively change the wing kinematics to produce aerodynamic moments. However, if the flight dynamics were dominated by damping, the amount of active control and the demand on the neural circuits could be reduced. Compared with yaw dynamics, which have been studied for the saccadic manoeuvres of flies (Bender and Dickinson, 2006a, b; Dickinson, 2005; Elzinga et al., 2012), understanding roll and pitch dynamics are more crucial for the analysis of overall flight stability (Sun, 2014). Thus, we explore the relative dominance of damping and inertia in roll and pitch manoeuvres.

If τ_a is close to τ_p, the active manoeuvring moment is comparable to the damping moment (i.e. acceleration is relatively small), and dynamics will be dominated by damping; accordingly, τ_{CL} will be greater than either τ_a or τ_p. If τ_a is less than half of τ_p, the active manoeuvring moment is more than twice the damping moment, and the dynamics will dominated by inertia; accordingly, τ_{CL} will be less than τ_p, but greater than τ_a. Therefore, the relative dominance of damping and inertia can be readily inferred by comparing the values of the above three constants.

For pitch manoeuvres of magnificent hummingbirds, τ_a (9.1 ms) was considerably smaller than τ_p (69.7 ms), and τ_{CL} (33.6 ms) was between τ_a and τ_p (Tables 1 and 2). Thus, pitch dynamics were inertia-dominated. For roll manoeuvres of magnificent hummingbirds, τ_a (12.3 ms) was close to τ_p (10.9 ms), and τ_{CL} (38.1 ms) was much larger, indicating that roll dynamics were damping-dominated because active manoeuvring moment and damping moment were comparable. Similar patterns were apparent in the black-chinned hummingbird. This conclusion was consistent with statistical analysis of wing kinematics during the manoeuvres (Cheng et al., 2016), wherein we found that pitch angular rates and accelerations were strongly correlated with a

Table 3. Muscle mass-specific power of hummingbirds during hovering, pitching and rolling flight assuming perfect muscle elastic energy storage

	Hover	Pitch		Roll		
				P^*_{roll} (W kg^{-1})		
Species	P^*_{hover} (W kg^{-1})	P^*_{pitch} (W kg^{-1})	$\Delta n/n$ (%)	Left wing	Right wing	$\Delta n/n$ (%)
Magnificent hummingbird (*Eugenes fulgens*)	185, 216* [232, 253]	590 (219%) [500, 772]	47	881 (376%) [845, 1012]	592 (220%) [565, 794]	50
Black-chinned hummingbird (*Archilochus alexandri*)	228, 285* [208, 274]	482 (111%) [411, 647]	16	361 (58%) [436, 335]	292 (28%) [346, 325]	6

Muscle to body-mass ratios of magnificent hummingbird (27.1%) and black-chinned hummingbirds (29%) are obtained from Chai and Millard (1997). Increase in wingbeat frequency during manoeuvres is expressed as a percentage of hovering wingbeat frequency ($\Delta n/n$). For P^*_{hover}, values with an asterisk are calculated assuming zero muscle elastic energy storage (Ellington, 1984) and using inertial power estimated from Chai and Millard (1997). Zero and perfect muscle-elastic energy storage represent maximum and minimum estimates of required muscle mass-specific power, respectively. For P^*_{pitch} and P^*_{roll}, values in parentheses represent the percentage increase of power during pitch and roll relative to hovering, and values in square brackets represent the power calculated using nominal wing kinematics ±s.d. Note that owing to aerodynamic nonlinearities, these may not be centred on the mean.

Journal of Experimental Biology

Journal of Experimental Biology (2016) 219, 3532-3543 doi:10.1242/jeb.137570

number of wing kinematic variables. However, only roll angular rates were significantly correlated with wing kinematic variables, indicating that changes of wing motion during roll manoeuvre were proportional to angular velocity but not acceleration, a direct outcome of damping-dominated dynamics (Greeter and Hedrick, 2016; Springthorpe et al., 2012).

Performance limitation imposed by delays in neural sensing and control

Despite pitch and roll having different open-loop dynamics, in escape manoeuvres, the closed-loop performance about these two axes, as indicated by the closed-loop time constants (Tables 1, 2), was quite similar and the hummingbirds of both species were able to roll and pitch stably at similar rates (Cheng et al., 2016). Several studies have suggested that closed-loop performance and stability of a flying animal engaged in rapid manoeuvres are primarily limited by delays in the neural sensing and motor control systems (Chang and Wang, 2014; Fuller et al., 2014; Ristroph et al., 2013). Passive damping (such as that during yaw manoeuvres; Hedrick et al., 2009; Springthorpe et al., 2012) could potentially alleviate this demand of low latency in the animal's neural sensing and control systems. Therefore, it can be inferred from our results that roll and pitch manoeuvres of similar performance, but with different damping properties, may impose different requirements on an animal's neural sensing and control systems. We develop this argument more rigorously using a control-theoretic perspective.

Plotting the contour of τ_{CL} as a function of Δt and τ_c for magnificent and black-chinned hummingbirds (Fig. 5), with τ^*_{CL} represented by a blue curve, indicates the best closed-loop performance at each assumed delay Δt. The contour line of our empirically measured τ_{CL} (Tables 1, 2) is also plotted (Fig. 5), which specifies a boundary, out of which the closed-loop performance cannot be satisfied. The rightmost point of the boundary projected on the Δt axis indicates the largest allowable time delay. When delays increase, closed-loop performance degrades as expected, but more slowly in roll than in pitch. The optimal controller time constant τ^*_c (Fig. 5) also increases with the delays, indicating that a hummingbird could rely more on direct angular rate feedback than integrated angular position feedback in the presence of a large delay.

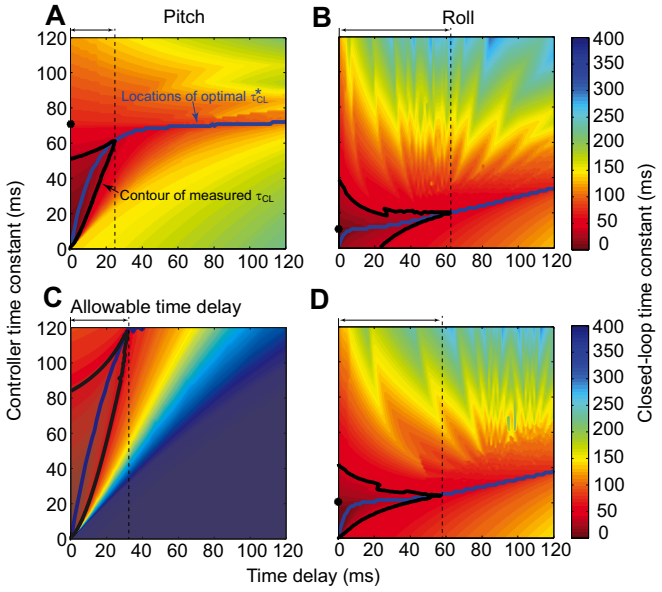

Fig. 5. Contour plots of closed-loop time constant as a function of assumed controller time constant and time delay of neural sensing and motor control. (A,B) Magnificent hummingbirds; (C,D) black-chinned hummingbirds. The lowest τ^*_{CL} (Eqn 22) for the fastest closed-loop response achievable is shown as a blue curve. The contour line of the measured τ_{CL} from actual manoeuvres specifies a boundary, out of which the closed-loop performance cannot be satisfied. The rightmost point of the boundary projected on the Δt axis indicates the largest allowable time delay for achieving the observed closed-loop performance. The range of the time delay tested (same for the controller constant) ranges from 0 to 120 ms, which covers the range of possible delays in a hummingbird's neural sensing (vision and proprioception) and motor control system. Filled circles on the ordinate represent the values of open-loop time constants τ_p.

In escape manoeuvres, pitch and roll had similar τ_{CL} (Tables 1, 2); however, they imposed different requirements on neural sensing and motor control (Fig. 5). The allowable time delay for roll dynamics is approximately 60 ms for both species, significantly greater than the escape reaction time of ~21 ms (magnificent hummingbird) and ~29 ms (black-chinned hummingbird) (Cheng et al., 2016), which is a coarse, conservative estimate of Δt. Thus, for roll manoeuvring, observed closed-loop performance can be achieved in the presence of potential delays using a PI controller. For pitch dynamics, allowable time delays are ~25 ms (magnificent hummingbird) and ~32 ms (black-chinned hummingbird) (Fig. 5A,C), only slightly higher than escape reaction times. This indicates that to achieve the observed closed-loop performance, the hummingbirds may have reached performance limitations imposed by the neural delay if it is close to the estimated reaction. Although the lack of accurate component-level information on the processing of the neural system prevents us from making firm conclusions, we infer that if the actual delay was longer than 30 ms, for example, in poor ambient light, the observed performance of pitch manoeuvring cannot be achieved with the assumed PI control, and a more sophisticated controller that requires higher neural computation, such as prediction using internal models of the flight dynamics (which has been found in insect flight; e.g. Mischiati et al., 2015), could have been used by the hummingbirds. The contour of measured τ_{CL} in Fig. 5 shows that pitch manoeuvring requires a greater controller time constant (and therefore relies more on rate feedback) than roll manoeuvring when delay increases. In summary, inertia-dominated pitch dynamics impose a more stringent demand on neural sensing and motor control than does damping-dominated roll dynamics. For similar closed-loop performance in executing a controlled manoeuvre, pitching can only tolerate half of the delay permitted for a roll manoeuvre.

Comparing the pitch performance of the two hummingbird species, black-chinned hummingbirds have slightly slower closed-loop dynamics and similar allowable time delays as magnificent hummingbirds (Table 1). However, they need to use significantly higher controller time constants τ_c (comparing Fig. 5A and C) because they have much slower pitch dynamics (larger τ_p in Table 1). Therefore, from Eqn 18, it can be inferred that the black-chinned hummingbirds may rely more on direct angular-rate feedback than do magnificent hummingbirds to achieve similar closed-loop performance.

Performance limitation imposed by muscle power

The flight performance of animals has been categorized into burst (anaerobic) and sustainable (aerobic) performance (Marden, 1994). In general, flying insects have no anaerobic capacity, and birds are able to achieve two to 2.5 times their aerobic power limit by relying on anaerobic metabolism (Ruben, 1991). The performance of burst flight is undoubtedly vital for hummingbirds, because, as estimated here, hummingbirds in escape flight were required to produce as

much as 4.5 times the power required during hovering. A muscle mass-specific power as high as 881 W kg^{-1} was found for magnificent hummingbirds (Table 3), substantially higher than for hovering. Thus, in addition to limitations imposed by sensorimotor delays, muscle power also likely limits the performance of escape or flight manoeuvrability in general. Nevertheless, because the bird only has to sustain at such a level of muscle power for one to three wingbeats, it is unknown whether this is indeed the highest anaerobic power the birds are able to achieve. In previous maximal load-lifting experiments (Chai and Millard, 1997), hummingbirds were able to sustain short burst flight with four times the power of hovering flight for >10 wingbeats. However, a key difference between the power in load-lifting flight and escape manoeuvres is that lifting relies mainly on increasing wingbeat amplitude while escaping relies on increases in both frequency and amplitude (Cheng et al., 2016). Our novel observation from manoeuvring indicates that hummingbirds are able to significantly increase their muscle contractile velocity at least for a couple of wingbeats. Notably, because of experimental limitations and the use of a simplified aerodynamic model derived from the work of Ellington (1984), the mass-specific powers estimated from load-lifting experiments are likely to be underestimates (p. 251–252 in Dudley, 2000). This assertion is supported by the agreement between our present estimates of mass-specific power and a recent CFD study (Song et al., 2014b), both of which arrived at substantially higher estimates of muscle mass-specific power than previously reported. In addition, note that the magnitude of total aerodynamic force was also increased substantially because the hummingbirds were accelerating linearly during the manoeuvres. The increase of the power was used to create both aerodynamic moment and force for angular and linear motion, which were coupled to each other in the escape manoeuvres. Therefore, it should be emphasized here that it was not only the body rotation but the escape manoeuvre as a whole that was likely limited by the muscle power.

Assumption of near-maximal escape performance

We assumed we elicited near-maximal escape performance of hummingbirds, such that the escape times approached some limit that a hummingbird needed to move certain distance away from the hover location with a desired change in heading. Load-lifting performance of hummingbirds (Altshuler et al., 2010a; Chai et al., 1997; Chai and Dudley, 1995; Marden, 1987) is considered to be limited predominantly by the maximal muscle power, stress and strain rate and plausibly by some unquantified aerodynamic and anatomical constraints (Dudley, 2000). Maximal load-lifting capacity is a useful predictor of aspects of manoeuvring including roll rate and overall complexity (Segre et al., 2015). The limits of the escape performance, however, may be even more perplexing than that of load-lifting, as they reside in the closed-loop control performance resulting from the interaction of many complex processes in muscle physiology, sensorimotor systems (e.g. vision and proprioceptive organs), aerodynamics and even high-level escape-trajectory planning in the brain. Therefore, to quantify the limits of escape flight or other manoeuvres, future studies may need to determine performance metrics of failure, such as minimum distance and/or time travelled before the birds are able to regain stability.

Interspecific differences of muscle power in rotational manoeuvres

Aerodynamic power estimates showed that the larger magnificent hummingbird generated significantly higher power during pitching and rolling phases of the escape manoeuvres compared with the smaller black-chinned hummingbird. Rotating at similar roll rates, larger species used much greater changes of wing kinematics and wingbeat frequency (Cheng et al., 2016). This suggests that larger species may need higher power reserves in major flight muscles to match the manoeuvrability of smaller species, which is probably critical in interspecific aerial competitions (Altshuler, 2006; Stiles and Wolf, 1970). As shown in the following, our observation of greater kinematic changes in larger species and subsequent estimates of aerodynamic power are consistent with the predictions based on the scaling of flight dynamics as well as with previous physiological studies of hummingbird flight muscle.

If hummingbirds of different sizes were to perform an escape manoeuvre of the same angular velocity and acceleration, how would the required wing kinematic changes and the mass-specific power scale with body size? In the rolling phase of the manoeuvre when the damping is dominant (Appendix):

$$\gamma_L \propto R^{1.15}, \quad (23)$$

$$P^*_{roll} \propto R^{1.85}, \quad (24)$$

where γ_L is an indicator of the magnitude of wing kinematic change during roll and R is wing length. Similarly, in the pitching phase of the manoeuvre when the inertia is dominant:

$$\gamma_M \propto R^{1.3}, \quad (25)$$

$$P^*_{pitch} \propto R^2, \quad (26)$$

where γ_M is an indicator of the magnitude of change in wing kinematics during pitch. The above scaling relationships predict, for pitch and roll, that larger species would require greater changes in wing kinematics and mass-specific power to achieve degrees of rotational manoeuvrability (at low flight speed) similar to those of smaller species. The former is consistent with the substantial increase in wingbeat frequency and greater changes in wing kinematics observed in larger species during the entire course of escape manoeuvres (Cheng et al., 2016), and the latter is consistent with our power calculation using these wing kinematics. The scaling would favour smaller species for higher rotational manoeuvrability if mass-specific power remains constant across species. However, larger species are capable of executing similar or even faster rotational manoeuvres than smaller species by producing higher mass-specific power than smaller species, at least during the short period of the escape manoeuvre. Here we did not consider linear manoeuvrability. Using similar calculations as in rotational dynamics (Appendix), larger species should require equal or less mass-specific power to achieve linear manoeuvrability similar to that of smaller species (results not shown).

The above conclusions, drawn from the perspectives of flight dynamics and aerodynamic power, raise significant questions in relation to current understanding of the muscle physiology of flying animals. Classical theory on the dynamics of muscle contraction (Dudley, 2000; Ellington, 1991) predicts that mass-specific power scales with wingbeat frequency and hence is greater for smaller species. Some studies using aerodynamic modelling of power output have suggested that mass-specific power instead is independent or scales moderately positively with increasing mass (Askew et al., 2001; Chai and Millard, 1997; Marden, 1994). In contrast, whole-body take-off performance scales negatively with increasing mass during maximal take-off in Galliformes (Tobalske and Dial, 2000) and Corvidae (Jackson and Dial, 2011). Recent analysis of load-lifting capacity hummingbirds similarly suggests that muscle mass-specific power scales negatively with mass (Altshuler et al., 2010a). Negative scaling of available mass-specific

Journal of Experimental Biology (2016) 219, 3532-3543 doi:10.1242/jeb.137570

power may be partially offset by muscle strain, stress, fibre type or motor-unit recruitment such that it is less negative than the scaling of wingbeat frequency (Jackson and Dial, 2011; Tobalske, 1996; Tobalske and Dial, 2000). However, elucidating the physiological mechanisms responsible for elevated mass-specific power we estimate larger species in the present study will require *in vivo* measures (Jackson et al., 2011; Tobalske et al., 2003) that are particularly challenging in hummingbirds (Tobalske et al., 2010).

An alternative hypothesis is that performance of the larger hummingbirds was closer to their maximum limit compared with the smaller species because of differences in behavioural motivation (i.e. the larger hummingbirds were trying harder). This hypothesis could be tested using behavioural experiments to measure relative fear or risk assessment (Stankowich and Blumstein, 2005). Uncertainty about physiological and behavioural mechanisms permitting the phenomenal performance of hummingbirds signals the need for continued study of the ecological and evolutionary demands for manoeuvrability during foraging, aerial competitions and escape in habitat shared by large and small hummingbird species.

APPENDIX

Body moment of inertia and centre of mass

Body moments of inertia (MOIs) of magnificent and black-chinned hummingbirds are shown in Table A1. They were estimated based on computer models (in SolidWorks, Waltham, MA, USA) for each species using measured morphological and mass properties from Cheng et al. (2016). Each model species was composed of seven parts: head, neck, torso, left wing, right wing, tail and undertail coverts. The shape profiles and dimensions of each part were extracted from the high-speed video images of the hovering birds. To ensure the accuracy of the model dimensions, we compared major dimensional parameters extracted from the video images with our direct measurements of the birds (see table 1 in Cheng et al., 2016). The relative mass ratio of each body part to the total body mass was estimated by dissecting and weighing a previously frozen calliope hummingbird (*Selasphorus calliope*, 3 g) carcass. We assumed that relative masses were constant in all the model species, except for the black-chinned hummingbird, the direct measurements of which revealed a relatively wider abdomen than the other species. The mass of each body part for our study species was then estimated based on its mass ratio and the total measured body mass, and its density was calculated by dividing the mass by its volume, under the assumption of uniform density. The mass of the black-chinned hummingbird's torso was estimated based on the torso density of the broad-billed hummingbird. Because the neck has a much lower density compared with other body parts, its density was assumed to be identical to that of the wing, and so was the tail. The remaining portion of the total mass was assigned to the undertail coverts. The density of the undertail coverts was the lowest among all body parts; therefore, we were compelled to separately model the body and the undertail coverts for better estimation of the MOIs and centre of mass. Finally, the MOIs and the location of the centre of mass for each model species were calculated using SolidWorks while setting the wings to their postures at the middle of each half stroke.

Table A1. Moments of inertia (MOIs) of hummingbird models calculated using SolidWorks models based on measured morphology

Species	I^{b}_{xx} roll	I^{b}_{yy} pitch	I^{b}_{zz} yaw	I^{s}_{xx} roll	I^{s}_{zz} yaw	I^{s}_{xz} roll and yaw
Magnificent hummingbird (*Eugenes fulgens*)	958	2119	2741	2004	1694	878
Black-chinned hummingbird (*Archilochus alexandri*)	183	483	577	414	346	194

Superscript 'b' represents the MOIs with respect to the body principal coordinate frame and 's' represents the MOIs relative to the stroke-plane coordinate frame (for definition of coordinate frames, see fig. 1 in Cheng et al., 2016). All units are g mm^2. I^{s}_{xz} is the roll and yaw product of inertia.

Scaling of wing kinematics and mass-specific power

Here we estimate the magnitude of wing kinematic change and the pertinent aerodynamic power assuming the birds of different species are performing rotational manoeuvres with constant angular velocity and/or acceleration. Because the roll and pitch dynamics have different characteristics, they will be treated separately.

Roll dynamics

As shown in the Results, the roll dynamics is dominated by damping, which is proportional to angular velocity. Therefore, neglecting the acceleration, the stroke-averaged roll moment produced by the active change in wing kinematics (L_a) approximately balances the stroke-averaged passive damping due to flapping counter torque (L_p). L_a and L_p can be estimated by the following equations based on the quasi-steady aerodynamic model (also refer to Cheng and Deng, 2011; Hedrick et al., 2009):

$$L_a = \gamma_L \frac{\hat{C}^L_a \rho R^4 \bar{c} \hat{r}_3^3 (S) \Phi^2 n^2}{8}, \quad \text{(A1)}$$

$$L_p = \hat{C}^L_p \rho R^4 \bar{c} \hat{r}_3^3 (S) \Phi n p, \quad \text{(A2)}$$

where Φ and n are wingbeat amplitude and frequency, respectively; the factor γ_L represents a temporary change in the roll torque generated by the wing owing to a lumped effect of wing kinematic changes, without specifying the underlying mechanisms of change; p is roll rate; and $\hat{C}^L_a$ and $\hat{C}^L_p$ are dimensionless stroke-averaged constants that depend on the force coefficients and wing kinematics, both of which are assumed to be the same across different species. Letting L_p=L_a results in:

$$\gamma_L = \frac{8\hat{C}^L_p}{\hat{C}^L_a \Phi n} p \propto \frac{p}{n} \propto pR^{1.15}, \quad \text{(A3)}$$

where we have assumed that the wingbeat amplitude and the value of $nR^{1.15}$ both remain constant across species (see table 2 in the companion paper, Cheng et al., 2016). In addition, using scaling of hummingbird wing length with respect to body mass, $R \propto m^{0.5}$ (Greenewalt, 1962), and constant muscle-to-body mass ratio (see Table 3 footnotes), the mass-specific power required for the roll rotation can be estimated by:

$$P^*_{roll} = L_p p / m_{muscle} \propto R^3 n p^2 \propto p^2 R^{1.85}. \quad \text{(A4)}$$

Pitch dynamics

During pitch rotation, the dynamics is dominated by inertia; therefore, if neglecting the damping moment, the pitch acceleration can be calculated by:

$$\dot{q} = \frac{M_a}{I} = \gamma_M \frac{\hat{C}^M_a \rho R^4 \bar{c} \hat{r}_3^3 (S) \Phi^2 n^2}{8I}, \quad \text{(A5)}$$

Journal of Experimental Biology

where $\hat{C}_a^M$ is a dimensionless stroke-averaged constant similar to $\hat{C}_a^L$ and $\hat{C}_p^L$, and the factor γ_M has a definition similar to that of γ_L. With the same assumptions made in roll dynamics, the above equation leads to the magnitude of wing kinematic change:

$$\gamma_M \propto \frac{\dot{q}}{n^2} \propto \dot{q}R^{1.3}. \quad \text{(A6)}$$

Next, without damping, and assuming the scaling of wing length, the multiplication of active torque and angular velocity yields the mass-specific power:

$$P^*_{\text{pitch}} = \frac{M_a q}{m_{\text{muscle}}} \propto \gamma_M R^3 n^2 \, q \propto \dot{q}qR^2. \quad \text{(A7)}$$

Acknowledgements
We thank the director and staff at the Southwestern Research Station (under the direction of the American Museum of Natural History, New York, USA) for hosting our research efforts. We also thank N. Cowan for discussion on modelling the delays in neural sensing and control.

Competing interests
The authors declare no competing or financial interests.

Author contributions
B.C., B.W.T., G.T.-C. and X.D. contributed to the design of experiments, B.C., B.W.T., D.R.P. and S.M.W. prepared the experiments, and B.C. and B.W.T. performed the experiments. All authors contributed to the interpretation of findings and preparation of the manuscript, Y.W. performed numerical simulation for damping acting on the body and tail, and B.C., B.W.T. and T.L.H. contributed to the data analysis.

Funding
Funding was provided by the National Science Foundation [NSF CMMI 1234737 to X.D., B.W.T. and T.L.H.] and the National Aeronautics and Space Administration [Climate and Biological Response 10-BIOCLIM10–0094 to D.R.P.].

Data availability

Supplementary information
Supplementary information available online at
http://jeb.biologists.org/lookup/doi/10.1242/jeb.137570.supplemental

References
Altshuler, D. L. (2006). Flight performance and competitive displacement of hummingbirds across elevational gradients. *Am. Nat.* **167**, 216-229.
Altshuler, D. L., Dudley, R., Heredia, S. and McGuire, J. A. (2010a). Allometry of hummingbird lifting performance. *J. Exp. Biol.* **213**, 725-734.
Altshuler, D. L., Welch, K. C., Cho, B. H., Welch, D. B., Lin, A. F., Dickson, W. B. and Dickinson, M. H. (2010b). Neuromuscular control of wingbeat kinematics in Anna's hummingbirds (*Calypte anna*). *J. Exp. Biol.* **213**, 2507-2514.
Altshuler, D. L., Quicazán-Rubio, E. M., Segre, P. S. and Middleton, K. M. (2012). Wingbeat kinematics and motor control of yaw turns in Anna's hummingbirds (*Calypte anna*). *J. Exp. Biol.* **215**, 4070-4084.
Askew, G. N., Marsh, R. L. and Ellington, C. P. (2001). The mechanical power output of the flight muscles of blue-breasted quail (*Coturnix chinensis*) during take-off. *J. Exp. Biol.* **204**, 3601-3619.
Beatus, T., Guckenheimer, J. M. and Cohen, I. (2015). Controlling roll perturbations in fruit flies. *J. R. Soc. Interface* **12**, 20150075.
Bender, J. A. and Dickinson, M. H. (2006a). A comparison of visual and haltere-mediated feedback in the control of body saccades in *Drosophila melanogaster*. *J. Exp. Biol.* **209**, 4597-4606.
Bender, J. A. and Dickinson, M. H. (2006b). Visual stimulation of saccades in magnetically tethered *Drosophila*. *J. Exp. Biol.* **209**, 3170-3182.
Chai, P. and Dudley, R. (1995). Limits to vertebrate locomotor energetics suggested by hummingbirds hovering in heliox. *Nature* **377**, 722-725.
Chai, P. and Millard, D. (1997). Flight and size constraints: hovering performance of large hummingbirds under maximal loading. *J. Exp. Biol.* **200**, 2757-2763.
Chai, P., Chen, J. S. and Dudley, R. (1997). Transient hovering performance of hummingbirds under conditions of maximal loading. *J. Exp. Biol.* **200**, 921-929.
Chang, S. and Wang, Z. J. (2014). Predicting fruit fly's sensing rate with insect flight simulations. *Proc. Natl. Acad. Sci. USA* **111**, 11246-11251.
Cheng, B. and Deng, X. (2011). Translational and rotational damping of flapping flight and its dynamics and stability at hovering. *IEEE Trans. Robot.* **27**, 849-864.
Cheng, B., Fry, S. N., Huang, Q. and Deng, X. (2010). Aerodynamic damping during rapid flight maneuvers in the fruit fly *Drosophila*. *J. Exp. Biol.* **213**, 602-612.
Cheng, B., Deng, X. and Hedrick, T. L. (2011). The mechanics and control of pitching manoeuvres in a freely flying hawkmoth (*Manduca sexta*). *J. Exp. Biol.* **214**, 4092-4106.
Cheng, B., Tobalske, B. W., Powers, D. R., Hedrick, T. L., Wethington, S. M., Chiu, G.T.-C. and Deng, X. (2016). Flight mechanics and control of escape manoeuvres in hummingbirds. I. Flight kinematics. *J. Exp. Biol.* **219**, 3518-3531.
Clark, C. J. (2009). Courtship dives of Anna's hummingbird offer insights into flight performance limits. *Proc. R. Soc. B Biol. Sci.* **276**, 3047-3052.
Clark, C. J. (2011). Effects of tail length on an escape maneuver of the red-billed streamertail. *J. Ornithol.* **152**, 397-408.
Clark, C. J., Feo, T. J. and Escalante, I. (2011). Courtship displays and natural history of scintillant (*Selasphorus scintilla*) and volcano (*S. flammula*) hummingbirds. *Wilson J. Ornithol.* **123**, 218-228.
Cowan, N. J., Lee, J. and Full, R. J. (2006). Task-level control of rapid wall following in the American cockroach. **209**, 3043.
Cowan, N. J., Ankarali, M. M., Dyhr, J. P., Madhav, M. S., Roth, E., Sefati, S., Sponberg, S., Stamper, S. A., Fortune, E. S. and Daniel, T. L. (2014). Feedback control as a framework for understanding tradeoffs in biology. *Integr. Comp. Biol.* **54**, 223-237.
Dickinson, M. H. (2005). The initiation and control of rapid flight maneuvers in fruit flies. *Integr. Comp. Biol.* **45**, 274-281.
Dickinson, M. H., Lehmann, F.-O. and Chan, W. P. (1998). The control of mechanical power in insect flight. *Am. Zool.* **38**, 718-728.
Dickinson, M. H., Lehmann, F.-O. and Sane, S. P. (1999). Wing rotation and the aerodynamic basis of insect flight. *Science* **284**, 1954-1960.
Dickson, W. B., Straw, A. D., Poelma, C. and Dickinson, M. H. (2006). An integrative model of insect flight control. In *Proceedings of the 44th AIAA Aerospace Sciences Meeting and Exhibit*, pp. 31-38. American Institute of Aeronautics and Astronautics.
Dudley, R. (2000). *The Biomechanics of Insect Flight*. Princeton, NJ: Princeton University Press.
Ellington, C. P. (1984). The aerodynamics of hovering insect flight. VI. lift and power requirements. *Philos. Trans. R. Soc. Lond. B Biol. Sci.* **305**, 145-181.
Ellington, C. (1985). Power and efficiency of insect flight muscle. *J. Exp. Biol.* **115**, 293-304.
Ellington, C. (1991). Limitations on animal flight performance. *J. Exp. Biol.* **160**, 71-91.
Elzinga, M. J., Dickson, W. B. and Dickinson, M. H. (2012). The influence of sensory delay on the yaw dynamics of a flapping insect. *J. R. Soc. Interface* **9**, 1685-1696.
Flanagan, J. R. and Wing, A. M. (1997). The role of internal models in motion planning and control: evidence from grip force adjustments during movements of hand-held loads. *J. Neurosci.* **17**, 1519-1528.
Franklin, G. F., Powell, J. D. and Emami-Naeini, A. (1994). *Feedback Control of Dynamics Systems*. Reading, MA: Addison-Wesley.
Fry, S. N., Sayaman, R. and Dickinson, M. H. (2003). The aerodynamics of free-flight maneuvers in *Drosophila*. *Science* **300**, 495-498.
Fry, S. N., Sayaman, R. and Dickinson, M. H. (2005). The aerodynamics of hovering flight in *Drosophila*. *J. Exp. Biol.* **208**, 2303-2318.
Fuller, S. B., Straw, A. D., Peek, M. Y., Murray, R. M. and Dickinson, M. H. (2014). Flying *Drosophila* stabilize their vision-based velocity controller by sensing wind with their antennae. *Proc. Natl. Acad. Sci. USA* **111**, E1182-E1191.
Goller, B. and Altshuler, D. L. (2014). Hummingbirds control hovering flight by stabilizing visual motion. *Proc. Natl. Acad. Sci. USA* **111**, 18375-18380.
Greenewalt, C. H. (1962). Dimensional relationships for flying animals. *Smithson. Misc. Collect.* **144**, 1-46.
Greeter, J. S. and Hedrick, T. L. (2016). Direct lateral maneuvers in hawkmoths. *Biol. Open* **5**, 72-82.
Hedrick, T. L., Cheng, B. and Deng, X. (2009). Wingbeat time and the scaling of passive rotational damping in flapping flight. *Science* **324**, 252-255.
Hesselberg, T. and Lehmann, F.-O. (2007). Turning behaviour depends on frictional damping in the fruit fly *Drosophila*. *J. Exp. Biol.* **210**, 4319-4334.
Iwaniuk, A. N. and Wylie, D. R. W. (2007). Neural specialization for hovering in hummingbirds: hypertrophy of the pretectal nucleus lentiformis mesencephali. *J. Comp. Neurol.* **500**, 211-221.
Jackson, B. E. and Dial, K. P. (2011). Scaling of mechanical power output during burst escape flight in the Corvidae. *J. Exp. Biol.* **214**, 452-461.
Jackson, B. E., Tobalske, B. W. and Dial, K. P. (2011). The broad range of contractile behaviour of the avian pectoralis: functional and evolutionary implications. *J. Exp. Biol.* **214**, 2354-2361.
Leishman, J. G. (2006). *Principles of Helicopter Aerodynamics*. New York: Cambridge University Press.
Lentink, D. and Dickinson, M. H. (2009). Rotational accelerations stabilize leading edge vortices on revolving fly wings. *J. Exp. Biol.* **212**, 2705-2719.
Marden, J. H. (1987). Maximum lift production during takeoff in flying animals. *J. Exp. Biol.* **130**, 235-258.
Marden, J. H. (1994). From damselflies to pterosaurs: how burst and sustainable flight performance scale with size. *Am. J. Physiol.* **266**, R1077-R1077.

Miller, L. A., Goldman, D. I., Hedrick, T. L., Tytell, E. D., Wang, Z. J., Yen, J. and Alben, S. (2012). Using computational and mechanical models to study animal locomotion. *Integr. Comp. Biol.* **52**, 553-575.
Mischiati, M., Lin, H.-T., Herold, P., Imler, E., Olberg, R. and Leonardo, A. (2015). Internal models direct dragonfly interception steering. *Nature* **517**, 333-338.
Muijres, F. T., Elzinga, M. J., Melis, J. M. and Dickinson, M. H. (2014). Flies evade looming targets by executing rapid visually directed banked turns. *Science* **344**, 172-177.
Muijres, F. T., Elzinga, M. J., Iwasaki, N. A. and Dickinson, M. H. (2015). Body saccades of Drosophila consist of stereotyped banked turns. *J. Exp. Biol.* **218**, 864-875.
Nabawy, M. R. A. and Crowther, W. J. (2014). On the quasi-steady aerodynamics of normal hovering flight part II: model implementation and evaluation. *J. R. Soc. Interface* **11**, 20131197.
Reichardt, W. and Poggio, T. (1976). Visual control of orientation behaviour in the fly: part I. A quantitative analysis. *Q. Rev. Biophys.* **9**, 311-375.
Ristroph, L., Bergou, A. J., Ristroph, G., Coumes, K., Berman, G. J., Guckenheimer, J., Wang, Z. J. and Cohen, I. (2010). Discovering the flight autostabilizer of fruit flies by inducing aerial stumbles. *Proc. Natl. Acad. Sci. USA* **107**, 4820-4824.
Ristroph, L., Ristroph, G., Morozova, S., Bergou, A. J., Chang, S., Guckenheimer, J., Wang, Z. J. and Cohen, I. (2013). Active and passive stabilization of body pitch in insect flight. *J. R. Soc. Interface* **10**, 20130237.
Roth, E., Reiser, M. B., Dickinson, M. H. and Cowan, N. J. (2012). A task-level model for optomotor yaw regulation in *Drosophila melanogaster*: a frequency-domain system identification approach. In *Proceedings of the Conference on Decisions and Controls (CDC)*, Maui, Hawaii, pp. 3721-3726. Institute of Electrical and Electronics Engineers.
Ruben, J. (1991). Reptilian physiology and the flight capacity of *Archaeopteryx*. *Evolution* **45**, 1-17.
Sane, S. P. and Dickinson, M. H. (2002). The aerodynamic effects of wing rotation and a revised quasi-steady model of flapping flight. *J. Exp. Biol.* **205**, 1087-1096.
Sedov, L. I. (1965). *Two Dimensional Problems in Hydrodynamics and Aerodynamics*. New York: Interscience Publishers.
Segre, P. S., Dakin, R., Zordan, V. B., Dickinson, M. H., Straw, A. D. and Altshuler, D. L. (2015). Burst muscle performance predicts the speed, acceleration, and turning performance of Anna's hummingbirds. *ELife* **4**, e11159.
Sholtis, K. M., Shelton, R. M. and Hedrick, T. L. (2015). Field flight dynamics of hummingbirds during territory encroachment and defense. *PLoS ONE* **10**, e0125659.
Song, J., Luo, H. and Hedrick, T. L. (2014a). Comparison of CFD and quasi-steady analysis of hovering aerodynamics for a ruby-throated hummingbird. In *32nd AIAA Applied Aerodynamics Conference*. American Institute of Aeronautics and Astronautics.
Song, J., Luo, H. and Hedrick, T. L. (2014b). Three-dimensional flow and lift characteristics of a hovering ruby-throated hummingbird. *J. R. Soc. Interface* **11**, 20140541.
Springthorpe, D., Fernández, M. J. and Hedrick, T. L. (2012). Neuromuscular control of free-flight yaw turns in the hawkmoth Manduca sexta. *J. Exp. Biol.* **215**, 1766-1774.
Stankowich, T. and Blumstein, D. T. (2005). Fear in animals: a meta-analysis and review of risk assessment. *Proc. R. Soc. B Biol. Sci.* **272**, 2627-2634.
Stiles, F. G. (1982). Aggressive and courtship displays of the male Anna's hummingbird. *Condor* **84**, 208-225.
Stiles, F. G. and Wolf, L. L. (1970). Hummingbird territoriality at a tropical flowering tree. *The Auk* **87**, 467-491.
Sun, M. (2014). Insect flight dynamics: stability and control. *Rev. Mod. Phys.* **86**, 615-646.
Sun, M. and Tang, J. (2002). Lift and power requirements of hovering flight in *Drosophila virilis*. *J. Exp. Biol.* **205**, 2413-2427.
Taha, H. E., Hajj, M. R. and Beran, P. S. (2014). State-space representation of the unsteady aerodynamics of flapping flight. *Aerosp. Sci. Technol.* **34**, 1-11.
Tobalske, B. W. (1996). Scaling of muscle composition, wing morphology, and intermittent flight behavior in woodpeckers. *The Auk* **113**, 151-177.
Tobalske, B. W. and Dial, K. P. (2000). Effects of body size on take-off flight performance in the Phasianidae (Aves). *J. Exp. Biol.* **203**, 3319-3332.
Tobalske, B. W., Hedrick, T. L., Dial, K. P. and Biewener, A. A. (2003). Comparative power curves in bird flight. *Nature* **421**, 363-366.
Tobalske, B. W., Biewener, A. A., Warrick, D. R., Hedrick, T. L. and Powers, D. R. (2010). Effects of flight speed upon muscle activity in hummingbirds. *J. Exp. Biol.* **213**, 2515-2523.
Usherwood, J. R. and Ellington, C. P. (2002). The aerodynamics of revolving wings I. Model hawkmoth wings. *J. Exp. Biol.* **205**, 1547-1564.
Wang, Z. J., Birch, J. M. and Dickinson, M. H. (2004). Unsteady forces and flows in low Reynolds number hovering flight: two-dimensional computations vs robotic wing experiments. *J. Exp. Biol.* **207**, 449-460.
Warrick, D. R., Bundle, M. W. and Dial, K. P. (2002). Bird maneuvering flight: blurred bodies, clear heads. *Integr. Comp. Biol.* **42**, 141-148.
Warrick, D. R., Tobalske, B. W. and Powers, D. R. (2005). Aerodynamics of the hovering hummingbird. *Nature* **435**, 1094-1097.
Whitney, J. P. and Wood, R. J. (2010). Aeromechanics of passive rotation in flapping flight. *J. Fluid Mech.* **660**, 197-220.
Wolpert, D. M. and Ghahramani, Z. (2000). Computational principles of movement neuroscience. *Nat. Neurosci.* **3**, 1212-1217.